Published online 28 December 2012 *Nucleic Acids Research, 2013, Vol. 41, No. 4* **2709–2722**
doi:10.1093/nar/gks1328

A dual-site simultaneous binding mode in the interaction between parallel-stranded G-quadruplex $[d(TGGGGT)]_4$ and cyanine dye 2,2′-diethyl-9-methyl-selenacarbocyanine bromide

Wei Gai[1,2], Qianfan Yang[1,*], Junfeng Xiang[1], Wei Jiang[1], Qian Li[1], Hongxia Sun[1,2], Aijiao Guan[1,2], Qian Shang[1], Hong Zhang[1] and Yalin Tang[1,*]

[1]Beijing National Laboratory for Molecular Sciences (BNLMS), Center for Molecular Sciences, State Key Laboratory for Structural Chemistry for Unstable and Stable Species, Institute of Chemistry, Chinese Academy of Sciences (ICCAS), Beijing 100190, PR China and [2]Department of Chemistry, University of Chinese Academy of Sciences, Beijing 100049, PR China

Received August 31, 2012; Revised November 24, 2012; Accepted November 26, 2012

ABSTRACT

G-quadruplexes have attracted growing attention as a potential cancer-associated target for both treatment and detection in recent years. For detection purpose, high specificity is one of the most important factors to be considered in G-quadruplex probe design. It is well known that end stacking and groove binding are two dominated quadruplex-ligand binding modes, and currently most reported G-quadruplex probes are designed based on the former, which has been proven to show good selectivity between quadruplexes and non-quadruplexes. Because groove of G-quadruplex also has some unique chemical properties, it could be inferred that probes that can interact with both the groove and G-tetrad site of certain G-quadruplexes simultaneously might possess higher specificity in aspects of discriminating different quadruplexes. In this article, we report a cyanine dye as a potential novel probe scaffold that could occupy both the 5′-end external G-tetrad and the corresponding groove of the G-quadruplex simultaneously. By using various spectrum and nuclear magnetic resonance techniques, we give a detailed binding characterization for this dual-site simultaneous binding mode. A preliminary result suggests that this mode might provide highly specific recognition to a parallel-stranded G-quadruplex. These findings and the structural elucidation might give some clues in aspects of developing highly specific G-quadruplex probes.

INTRODUCTION

When DNA actively participates in biological processes, including replication, transcription and recombination, it can form a special secondary conformation termed G-quadruplex (1–3). G-quadruplex is stabilized by Hoogsteen hydrogen bonding among four guanine bases arranged in a square planar configuration, the so-called G-quartets. The secondary structure of G-quadruplex was characterized *in vitro* in the presence of monovalent cations such as K^+ or Na^+ (4). Many studies in the past two decades revealed that G-rich tracts capable of forming the G-quadruplex motif are widespread in the genome, such as telomeres (5) and promoter regions of several important oncogenes (6). These G-rich sequences are implicated in cancer cell proliferation (7,8), so G-quadruplex motifs are attracting more and more interest. On one hand, the ligands that are able to stabilize or regulate the formation of specific G-quadruplex motifs are emerging as potential anticancer therapeutics (9–11). On the other hand, highly specific verification of G-quadruplex motifs is considered as a potential cancer detection approach (12,13). For both treatment and detection purposes, specific recognition of the G-quadruplexes from other DNA motifs, such as single-stranded or double-stranded DNA, is a foundational task in aspects of developing functional G-quadruplex ligands.

*To whom correspondence should be addressed. Tel: +86 1 08 26 17 304; Fax: +86 1 06 25 22 090; Email: tangyl@iccas.ac.cn
Correspondence may also be addressed to Qianfan Yang. Tel: +86 10 62558322; Fax: +86 10 62522090; Email: yangqf@iccas.ac.cn

To date, two main binding modes between G-quadruplex DNAs and their ligands have been well documented: the end-stacking and the groove-embedding mode. Most G-quadruplex binders reported so far adopt the end-stacking mode, such as porphyrins (14,15), telomestatin (9,16), cyanine dyes (13), quinazoline derivatives (17), oxazole-containing macrocycles (18) and quercetin (19). The reported groove binders include distamycin-A (20,21), diarylethynylamides (22) and BMVC (23,24), which are obviously fewer in number than the end-stacking binders.

Because a number of G-quadruplex sequences may exist simultaneously within a genome, it is a challenge for chemists to discriminate specific G-quadruplexes in the presence of double-stranded DNA, as well as other G-quadruplex motifs. The most remarkable difference between G-quadruplex and double-stranded DNA is the G-tetrad composed of four guanine bases. It is well known that the external G-tetrad is a key target for designing probes that could well discriminate G-quadruplex from duplex (25). However, probes that could discriminate a specific G-quadruplex motif from diverse G-quadruplexes have undergone limited study. It has been reported that G-quadruplex groove recognition offers the potential for the enhanced selectivity among various G-quadruplexes (26). Thus, it could be rationally inferred that the dual-site simultaneous binding ligands, which can bind to G-quadruplex on the terminal G-quartet and the groove of G-quadruplex at the same time, are likely to be highly specific probes. Unfortunately, such kind of ligand is rarely reported. The only case at this strategy is the modified distamycin-A, which is found to be able to simultaneously bind to the G-tetrad and groove of a parallel-stranded G-quadruplex (27).

Cyanine dyes were found to be applicable in the study of various biological systems owing to their specific photochemical properties (28,29). We reported previously a supramolecular cyanine dye ETC could assemble to aggregates in phosphate buffered saline (PBS) and end-stack on the terminal G-tetrad of specific G-quadruplexes in the form of monomer (13,30). The high specificity of ETC makes it an excellent G-quadruplex structural probe. In this article, we report an analog of cyanine dye ETC, 2,2′-diethyl-9-methyl-selenacarbocyanine bromide (termed DMSB, shown in Figure 1a). The major change of the structure is replacement of the naphthothiazole scaffold by the benzoselenazole unit, as well as the removal of the cationic sulfo group from the *N*-alkyl chains. Owing to the structural change, DMSB is capable of binding to the intermolecular parallel G-quadruplex $[d(TGGGGT)]_4$ (abbreviated ***TG4T***), in the form of both monomer and dimer. Moreover, DMSB dimer could occupy the 5′-end terminal G-tetrad and the corresponding groove of ***TG4T*** simultaneously, which is the rare dual-site simultaneous binding mode.

Ultraviolet–visible (UV-vis) and fluorescence titration results suggest that there are two binding modes in the DMSB-***TG4T*** system: the monomer and the dimer binding. Further, the hydrogen-1 nuclear magnetic resonance (^{1}H-NMR) titration method was then used to determine the binding sites. For the complicated dimer binding, we designed several strategies to discuss its binding mode, which is finally proven as a dual-site simultaneous binding mode. At last, an NOE-restrained molecular dynamic simulation was performed to further present the detailed binding structure.

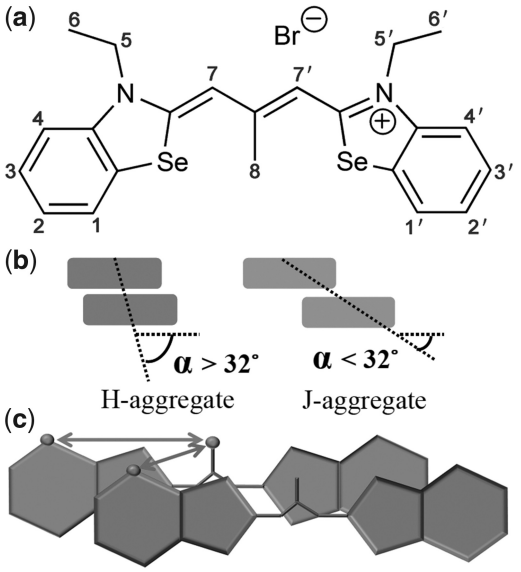

Figure 1. (**a**) The molecular structure of DMSB with renumbered protons. (**b**) Schematic representation of H- and J-aggregate dependent on the slippage angle α. (**c**) Schematic illustration for the NOE-based DMSB dimer.

MATERIALS AND EXPERIMENTS

Sample preparations

The cyanine dye DMSB was synthesized according to Hamer's and Brooker's methods (31,32), and the purity was evaluated by mass spectrometry and nuclear magnetic resonance. The synthesis of the oligonucleotides ***TG4T***, $[d(TGGGT)]_4$ (***TG3T***), $[d(TGGGGGGT)]_4$ (***TG6T***), $[d(TGGGGGGGGT)]_4$ (***TG8T***), $[d(TGG^{OMe}GGT)]_4$ and $[d(TGG^{Br}GGT)]_4$ was achieved following reported procedure (21). The two modified guanosines, 8-Br-phosphoramidite and 8-OMe-phosphoramidite, were directly purchased from Glen Research Corporation (Virginia, USA). Analytical grade methanol, KH_2PO_4, K_2HPO_4 and ethylenediaminetetraacetic acid (EDTA) were purchased from Beijing Chem. Co. (China). Ultrapure water was prepared by the Milli-Q Gradient ultrapure water system (Millipore).

The stock solutions of DMSB were prepared by dissolving it in methanol to 200 mM and then storing in the dark at −4°C. The stock solutions of oligonucleotides were prepared by dissolving them to phosphate buffer (20 mM KH_2PO_4/K_2HPO_4, 70 mM KCl, 1 mM EDTA, pH 7.4) followed by filtering through a microfiltration membrane ($\Phi = 0.22\,\mu m$). Then they were heated to 90°C for 5 min and gradually cooled to room temperature at a rate of 1°C min^{-1}. The concentrations of DNA stock solutions were determined by measuring their absorbance at 260 nm. All DNA samples were stored for more than

24 h at 4°C and then structurally identified by both circular dichroism (CD) and ^{1}H-NMR spectra.

UV-vis and fluorescence spectroscopic measurements

The UV-vis absorption spectra were measured by an Agilent-8453 spectrophotometer equipped with a Peltier effect heated cuvette holder in a 10-mm quartz cell. For melting experiments, the temperature rose from 30°C to 95°C at a heating rate of $1°C \cdot min^{-1}$ with a 3-min holding time before each measurement. Fluorescence spectra were taken on a Hitachi F-4500 spectrophotometer in a 10-mm quartz cell at room temperature. A xenon arc lamp was used in the excitation light source for fluorescence measurement. The excitation wavelength was 530 nm. Both excitation and emission slits were 5 nm, and the voltage was 400 V with a scan speed of $240 nm \cdot min^{-1}$.

CD spectra measurements

All the CD spectra were recorded on a JASCO J-815 spectrophotometer in a 10-mm quartz cell at room temperature. All spectra were collected with a scan speed of $500 nm \cdot min^{-1}$ and a response time of 0.5 s between 200 and 700 nm with five scans averaged. For melting experiments, the temperature rose from 30°C to 95°C at a heating rate of $1°C \cdot min^{-1}$ with a 3-min holding time before each measurement.

NMR experiments

The stock solution of DMSB for NMR experiments was prepared by dissolving 44.4 mg of DMSB in 1 ml of DMSO-d_6 (80 mM). The stock solution of ***TG4T*** was prepared by dissolving it in 0.5 ml of NMR buffer solution [20 mM KH_2PO_4/K_2HPO_4, 70 mM KCl, 0.2 mM EDTA, 90% H_2O/10% D_2O (v/v)] and then dialyzed through a bag with a cut-off molecular weight of 500 for 12 h to desalt. The ***TG4T*** samples was stored for >24 h at 4°C, and then the structures were identified by the CD spectra. The measured sample for ^{1}H NMR titration, TOCSY and phase-sensitive NOESY was prepared by mixing a certain volume of ***TG4T*** stock solution with DMSB stock solution. The final concentration of intermolecular ***TG4T*** G-quadruplex for each sample was 1.5 mM (6 mM for single-stranded ***TG4T***). The sample preparations of $[d(TGG^{OMe}GGT)]_4$ and $[d(TGG^{Br}GGT)]_4$ are generally identical to that of ***TG4T*** except that they were heated for 5 min at 90°C and slowly cooled to room temperature before adding DMSB to form the uniformly intermolecular G-quadruplex.

All NMR spectra were recorded on a Bruker Avance 600 spectrometer, which is equipped with a 5-mm BBI probe capable of delivering z-field gradients up to $50 G \cdot cm^{-1}$. The 1D chemical shifts were referred to that of 3-(trimethylsilyl)-propanoic acid. The 1D spectra were recorded by the standard Bruker pulse program p3919gp that applies 3–9–19 pulses with gradients for water suppression (33,34). The TOCSY spectrum (33) was recorded with a mixing time of 80 ms by using the mlevgpph19 sequences with a 3–9–19 pulsed-field gradient sequence for water suppression (33,34). Three NOESY spectra (35) were recorded with mixing times of 50, 100 and 200 ms, respectively. The noesygpph19 sequence with a 3–9–19 pulsed-field gradient sequence for H_2O suppression was used. Both TOCSY and NOESY spectra were recorded using the STATES-TPPI (36) procedure for quadrature detection with time domain data composed of 2048 complex points in F2 and 512 fids in the F1 dimension. All the experiments for both 1D and 2D were acquired using 128 scans for each spectrum with a relaxation delay of 2 s at 308 K. The NMR data were processed on a ThinkCenter M6300T workstation using FELIX 2004 software (Accelrys, San Diego, CA).

Structural study and energy calculation by molecular dynamics

The partial charges and structure of DMSB was calculated and optimized by Gaussian 03 using the DFT method with an HF/6-31G** basis set at the B3LYP level. Then the obtained atomic charges and structure of DMSB were subjected to molecular dynamics simulation. The sequence of G-quadruplex DNA ***TG4T*** was built by using Discovery Studio 3.1 (Accelrys, San Diego, CA).

The NOESY cross-peak volumes were fetched by FELIX 2004. The known fixed distance between G3-H2′ and G3-H2″ was used as the normalized scalar factor to convert peak volume to distance constraint. An S-M-W–type restraint bound was used, corresponding to strong NOEs ($1.0 < r_{ij} < 2.5$ Å), medium NOEs ($2.0 < r_{ij} < 4.0$ Å) and weak NOEs ($3.5 < r_{ij} < 6.0$ Å), respectively. Then the constraint file was generated by the FELIX program automatically containing 270 DNA-associated and 14 DNA-ligand distance constraints. Because the ***TG4T*** was a intermolecular parallel-stranded quadruplex, 64 hydrogen bonds among the guanines were manually added into the constraint file. In addition, 24 backbone torsion angles were used as dihedral constraints in the calculation, too. The guanine glycosidic torsion angle χ was limited in the range of $-100°/-160°$ to guarantee the anti-conformation of the guanines, which is characterized by parallel quadruplex. Other backbone torsion angles, such as α, β, γ, δ and ε, were not restrained to leave a sufficient flexibility space to the backbone to reach more accurate structures in subsequent dynamics simulation.

The molecular dynamics simulation works were performed by using Discovery Studio 3.1 on a ThinkCenter M6300T workstation under CHARMm forcefield. After the ligand was manually docked into the suitable position according to the spectral and NMR results, the DNA-ligand complex was solvated with a truncated octahedral box containing TIP3P water (37) whose boundary is 10 Å away from the complex with periodic boundary conditions being applied (38). The system was neutralized by adding 18 potassium ions. Then several equilibration steps were performed comprising minimization of the whole system (10 000 steps of steepest descent minimization followed by 50 000 steps of conjugated gradient minimization with DNA and ligand fixed) and slow heating to 300 K under NVT ensemble where Berendsen's weak coupling scheme (39) is used to achieve constant temperature. Then a 500-ps production procedure was carried out

in an isobaric-isothermal (NPT) ensemble, where the maintenance of the pressure and temperature was achieved based on the Nosé-Hoover method (40,41). The 12-Å cut-off radius was used for VDW interaction calculation, and the particle mesh Eward method (42) was used for electrostatic summation. For bonds containing hydrogen atoms, the SHAKE algorithm (43) is applied to constrain their motions. The equations of motion were integrated with the leapfrog algorithm (44). The force constants for NOE constraints were increased from 1 to 30 kcal·mol^{-1}·Å^{-2} during the first 5 ps and then maintained constant for the rest of the simulation. The simulation temperature was controlled ~300 K, and the time step was 1 fs. The conformation of the complex was saved every 100 fs. The produced trajectories were subjected to non-bond energy calculation by the Interaction Energy Calculation protocol, which is a protocol integrated in Discovery Studio used for non-bond interaction energy analysis (including the Van der Waals and Electrostatic energy) between two defined atom subsets, with the produced dynamic trajectories as input file. The protocol calculated the average Van der Waals energies with a non-bond cut-off distance of 10–12 Å and the electrostatic energies with an implicit distance-dependent dielectric constant of 1.0 between two defined atom groups from the last 100 ps of the produced dynamic trajectories.

RESULTS AND DISCUSSION

Spectral and assembly characteristics of dye DMSB

Formation of cyanine dye aggregates strongly depends on the specific structure of dyes, their concentrations and the medium (45,46). Aggregation of cyanine dyes usually takes place in polar solvent, such as aqueous solution (47,48). The UV-vis spectra of DMSB in both methanol and phosphate buffer (PBS) are shown in Supplementary Figure S1. In methanol, DMSB exhibits only one absorption band assigned to monomer (M-band) at ~554 nm, while in PBS, DMSB exhibits a primary absorption band at 554 nm assigned to monomer (M-band) (48), as well as a smaller shoulder peak ~512 nm assigned to dimer band (D-band) (47,49) according to the exciton model (50) and two reported DMSB analogs, DTC (51) and Cy3 (52). It is shown DMSB exists as an equilibrated mixture of monomers and dimers in PBS.

It is well known that cyanine dyes can aggregate in a face-to-face stacking way to form an H-dimer or in a head-to-tail arrangement to form a J-dimer (45), depending on the slippage angle α, the angle between the dye aggregation axis and the transition dipole moment. As shown in Figure 1b, dyes form H-aggregates (in a face-to-face stacking way) when $\alpha > 32^{o}$, whereas they form J-aggregates (in a head-to-tail stacking way) when $\alpha < 32^{o}$. The type of the aggregates could be easily determined by their absorption shifts to the corresponding monomer absorption band. H-aggregates lead to a hypsochromic shift while J-aggregates lead to a bathochromic shift. The hypsochromic shoulder peak ~512 nm indicates DMSB dimers here are H-dimers in PBS. Furthermore, the NOESY experiment (Supplementary Figure S1) proved that DMSB H-dimers exhibit a slight malposition of arrangement, rather than the exact face-to-face stacking in alignment (as shown in Figure 1c).

Interaction between DMSB and *TG4T*

TG4T is a truncated telomeric sequence from *Oxytricha* capable of forming a parallel-stranded G-quadruplex (53). Many G-rich tracts in the human genome can also form a parallel-stranded quadruplex, such as ***c-myc*** (54), ***c-kit*** (55) and telomeric DNA (56). Because the structure of ***TG4T*** has been well studied (57,58) and its NMR signal is relatively easy to identify, ***TG4T*** was chosen to perform the initial studies on the interaction between cyanine dye dimers and quadruplexes. The interaction of DMSB with ***TG4T*** was studied by gradually titrating ***TG4T*** (from 0.4 μM to 24 μM) to 12 μM DMSB. As shown in Figure 2a, the initial addition of ***TG4T*** causes a great increase of DMSB D-band absorbance accompanying with slight falling off of M-band (Figure 2b). This result suggests DMSB binds onto ***TG4T*** in the form of dimer. It indicates that ***TG4T*** is able to induce DMSB monomer to dimer when DMSB is in excess. With further addition of ***TG4T***, especially when the dye/DNA ratio is <3, the D-band absorbance starts to decrease with the rising of the M-band, indicating that induced DMSB dimers are disassembled to monomer with the further addition of DNA, which results in a lower dye/DNA stoichiometry. Thus, the DMSB behavior in the entire ***TG4T*** titration process can be divided into two stages: the stage of the dimer enhancement (D-mode stage) and the stage of the disassembling of dimer to monomer (M-mode stage). The two stages suggest that there are two different binding modes between the dye and DNA. It is also observed that the M-band of DMSB gradually shifts from 551 to 556 nm with the increase of ***TG4T***. This kind of bathochromic shift always infers the binding state of cyanine dye, caused by the higher refractive index of the macromolecular environment compared with that of water (59).

The corresponding fluorescence titration profiles of DMSB with ***TG4T*** were also examined to provide more spectral properties of the two stages. As shown in Figure 2a, in a high DMSB/***TG4T*** stoichiometry (>3), DMSB shows two weak and partially overlapped fluorescence emission bands at ~574 and 595 nm, assigned to bound monomer and dimer, respectively (Supporting Information, Supplementary Figure S2). Note that the relative position of the two bands in the fluorescence emission spectrum is opposite to that in the absorption spectrum. A similar phenomenon was also observed in the case of Cy3, an analog of DMSB, which has well proven the translocation of the dimer band in the fluorescence spectrum compared with that in the absorption spectrum in an AOT reverse micelles environment (52,60). Another interesting phenomenon is that the H-dimer of DMSB shows moderate fluorescence in the presence of ***TG4T***. Actually, it was reported that the fluorescence of cyanine dye H-aggregates is always strongly quenched and exhibits almost non-fluorescent in aqueous solution (49,61). In this case, the moderate

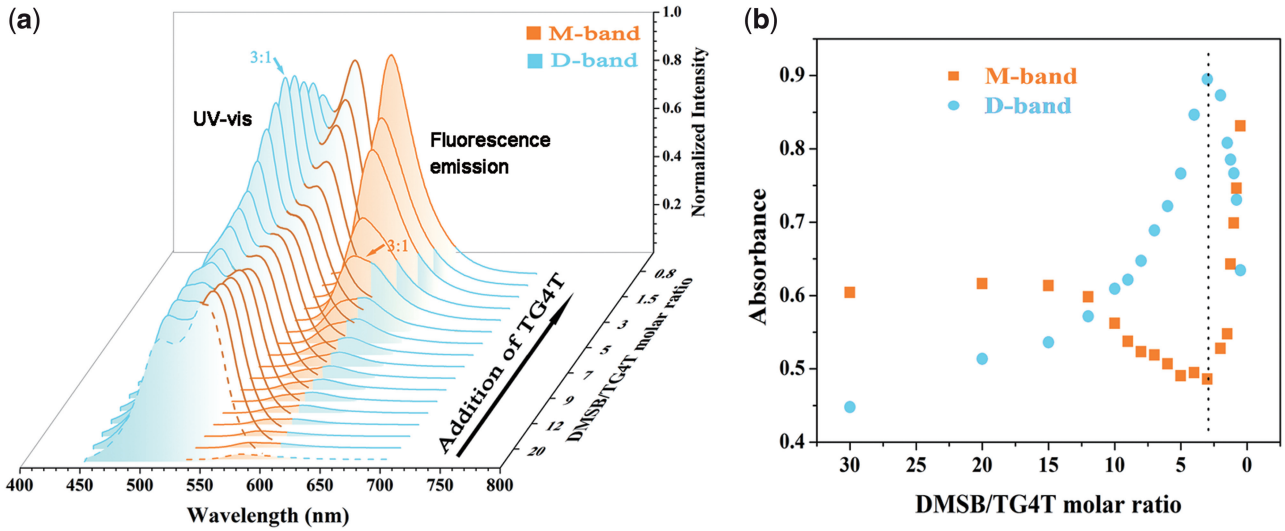

Figure 2. (**a**) The UV-Vis titration spectra (left) and corresponding fluorescence emission spectra (right) for 12 μM DMSB titrated with ***TG4T*** in PBS, where M-band and D-band are colored orange and light blue, respectively. (**b**) The variation of M-band and D-band of DMSB in absorbance as a function of the DMSB/***TG4T*** molar ratio.

fluorescence of DMSB H-dimer is most probably because the H-dimer exists in a rigid and confined environment (62), which further suggests the bound state of H-dimer. On the other hand, in a low DMSB/***TG4T*** molar ratio (<3), the fluorescence of DMSB monomer was strongly enhanced, which could be reasonably attributed to the restriction of radiationless deactivation of the excited singlet state for monomer when DMSB bound to ***TG4T***.

Based on the spectral results, it could be considered the interaction of DMSB with ***TG4T*** shows two concentration-related stages: DMSB monomer assembling to dimer, and dimer disassembling to monomer, corresponding to two different binding modes: D-mode and M-mode.

Binding site exploration for DMSB/TG4T

NMR is a powerful tool to study the binding sites in a host–guest interaction. We used ^{1}H-NMR titration to further explore the binding site between DMSB and ***TG4T***. Figure 3a shows the ^{1}H-NMR titration spectra of 0.5 mM ***TG4T*** with various concentrations of DMSB in PBS at 308 K. The ***TG4T*** resonance signals for the four imino protons (10–12 ppm), six aromatic protons (7–9 ppm) and two thymine methyl protons (1–2 ppm) were well resolved based on TOCSY, NOESY results and Randazzo's work (21).

Initial addition of DMSB to ***TG4T*** results in a relative low DMSB/***TG4T*** ratio (from 0.5:1 to 2:1), which is the M-mode stage. Clearly, the G5-NH, G5-H8, T6-H6 and T6-CH_3 signals (red peaks) of ***TG4T*** decrease and broaden sharply with the addition of DMSB, accompanying the remarkable upfield shift of G5-NH and G5-H8 signals, and the downfield shift of T6-H6 and T6-CH_3 ones. The resonance signals for T6-H6 almost disappear, which means an intermediate exchange. Figure 3b profiles the chemical shift's changes of each base proton during M-mode stage. The changes of the chemical shifts of G5 and T6 protons (>0.1 ppm) are much larger than those of others, suggesting the binding site for the DMSB monomer on ***TG4T*** is probably located between G5 and T6. It is reasonable because the G5 is 3′-terminal G-quartet and the DMSB monomer could stack between G5 and T6 through end-stacking mode, the most common binding mode of G-quadruplexes and their ligands.

Further titration resulted in a higher DMSB/***TG4T*** ratio (from 3:1 to 8:1), which is the D-mode stage. In Figure 3a, it can be seen that in this stage, the changes of the chemical shifts of the G5-NH, G5-H8, T6-H6 and T6-CH_3 signals (red peaks) are all almost invariable except that their shapes gradually recover and become sharp and narrow again. Such signal behaviors clearly indicate the saturation of the binding site between G5 and T6 on ***TG4T***. Moreover, the other three protons, G2-NH, G2-H8 and T1-CH_3 (blue peaks), start to exhibit a dramatic shift. Different with a slight upfield shift in M-mode, G2-NH, G2-H8 and T1-CH_3 signals broaden remarkably and exhibit a dramatic downfield shift. Besides, the chemical shift for G3-NH and G4-NH signals also changes from an up-field to down-field direction in this stage. Significantly different behavior of ^{1}H-NMR signals in D-mode stage indicated a totally different binding mode, rather than end-stacking in M-mode stage. Figure 3c presents the chemical shift's changes of each proton during D-mode stage. It could be seen that G2-NH signal changes significantly with a Δδ of ~0.3 ppm, followed by T1 and G3, whose Δδ are <0.1 ppm but still larger than those of G4, G5 and T6. This result shows a doubtless involvement of the G2 site and a possible involvement of T1 and G3 on D-mode binding. Apparently, DMSB turns out to be able to bind to another site around G2 on ***TG4T*** in this titration stage.

According to the ^{1}H-NMR titration results, the binding characterization of DMSB to ***TG4T*** is when [DMSB]/[***TG4T***] is <3, DMSB mainly end-stacks on G5 at the 3′-end of ***TG4T*** in the form of monomer, whereas with the increase of [DMSB]/[***TG4T***], DMSB starts to bind to

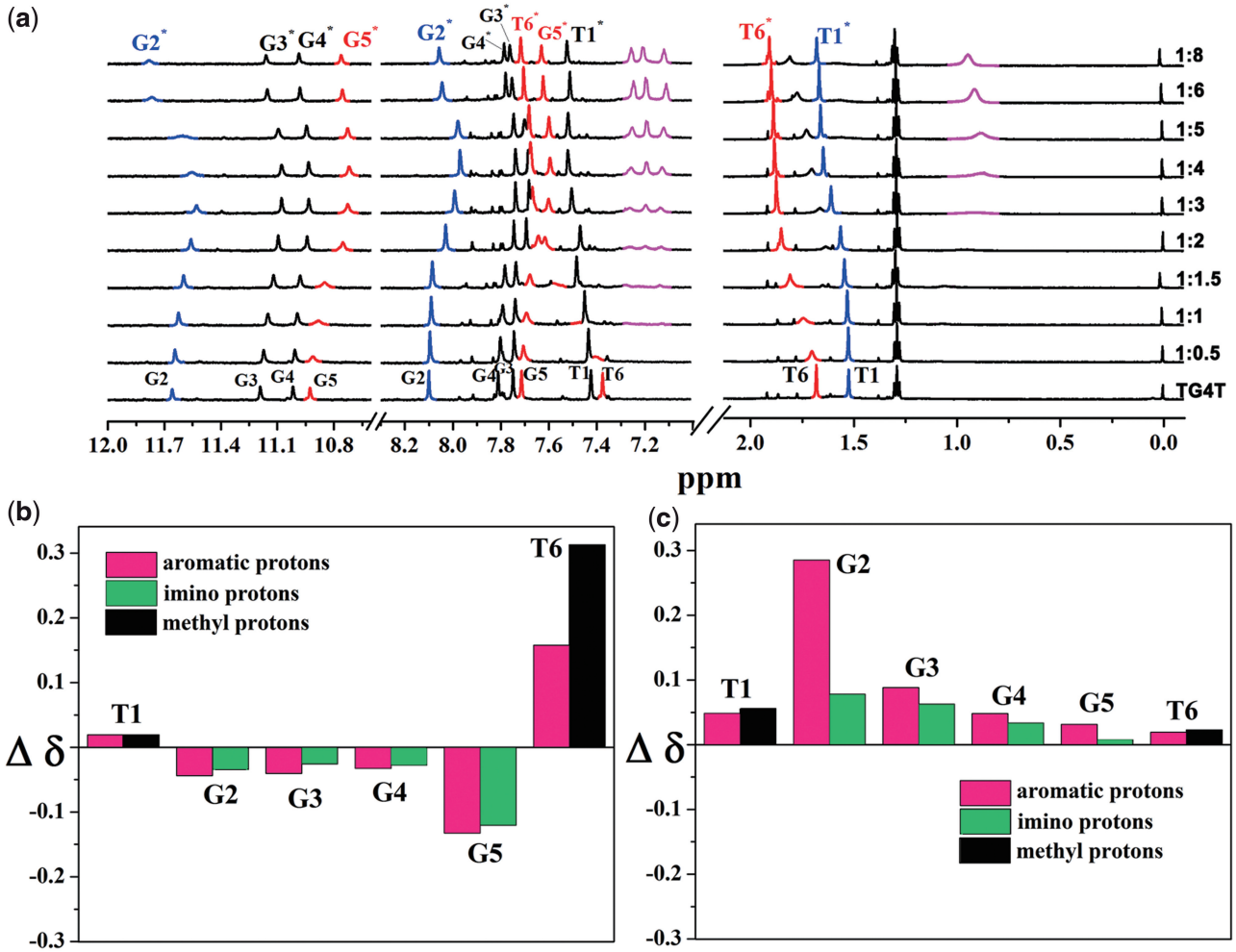

Figure 3. (**a**) The unambiguous assigned ^{1}H-NMR titration spectra of 0.5 mM ***TG4T*** (2 mM single-strand concentration) with different concentrations of DMSB (600 MHz, 308 K) in 0.4 mL phosphate buffer containing 20 mM KH_2PO_4/K_2HPO_4, 70 mM KCl, PH 7.4 (H_2O/D_2O 9:1, v/v). The ***TG4T***/DMSB molar ratios are shown along the right side of each spectrum. The magenta peaks indicate resonance signals of DMSB. Difference in chemical shifts (Δδ) of base protons on ***TG4T*** on binding of DMSB in (**b**) M-mode (complex of 1:2 ***TG4T***/DMSB ratio minus pure ***TG4T***) and (**c**) D-mode (complex of 1:8 ***TG4T***/DMSB ratio minus complex of 1:3 ***TG4T***/DMSB ratio). Δδ values are reported for aromatic (magenta), imino (green) and methyl (black) protons.

the second site near the G2 base at the 5′-end of ***TG4T*** in the form of dimer after the binding site between G5 and T6 is saturated. Judging from the ^{1}H-NMR results and the relative literature, the binding mode in M-mode stage is clear, whereas the precise binding mechanism for the D-mode stage still remains uncertain and needs further study.

Four possible dimer-binding modes of DMSB/*TG4T*

The UV and ^{1}H-NMR results explicitly provide two important pieces of information on the interaction between DMSB and ***TG4T*** in D-mode stage: the binding state of DMSB is dimer, and the binding site is around G2 of ***TG4T***. For the G-quadruplex structure, it is believed that there are three common binding sites: the external (end) G-tetrad, the quadruplex groove and the space between two G-tetrads. Based on the above experimental results and the possible binding sites on a G-quadruplex, four possible binding modes were proposed in D-mode stage (as shown in Figure 4). Mode (a) is characterized by one DMSB molecule intercalating between G2 and G3 tetrads while the other stacks on the G2 tetrad. Mode (b) is a pure end-stacking mode, whereas mode (c) is a pure groove occupation one. Mode (d) is a dual-site simultaneous binding mode in which DMSB dimer interacts with both the groove and the external G2 tetrad. Further experiments and discussions were performed to determine which mode is the most reasonable one.

Mode (a) can be excluded by exciton coupling theory

It is well known that the vertical separation between base pairs in duplex and that between G-tetrad layers in G-quadruplex are ~3.4 Å (63) and 3.1~3.4 Å (56), respectively. As is reported, the classical intercalator, ethidium bromide, can cause the structural perturbations of the DNA duplex and extends the vertical separation between the bases to 6.7 Å, almost doubling the separation (64). A study of the interaction between porphyrins and

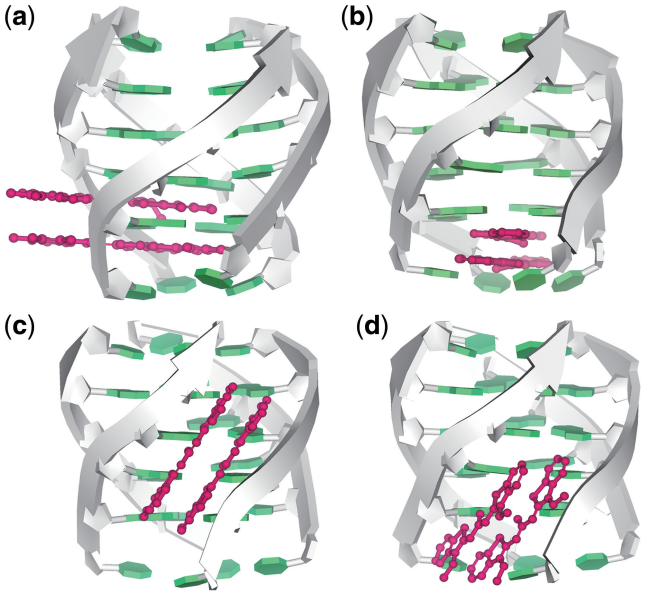

Figure 4. The proposed four possible binding modes of DMSB dimer to ***TG4T*** in D-mode stage: (**a**) partial-intercalation mode; (**b**) dimer end-stacking mode; (**c**) dimer groove occupying mode; (**d**) dual-site simultaneous binding mode.

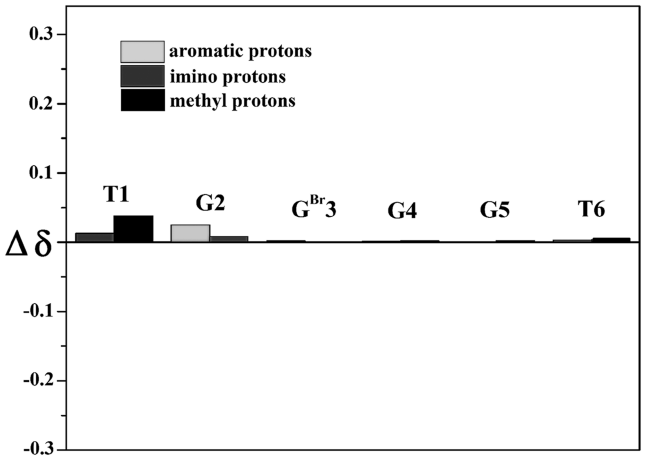

Figure 5. Difference in chemical shifts (Δδ) of protons on ***TG4T-Br*** bases on binding of DMSB during D-mode stage. Δδ values are calculated by complex of 1:8 ***TG4T-Br***/DMSB ratio minus complex 1:3 ***TG4T-Br***/DMSB ratio and are reported for aromatic (light grey), imino (dark grey) and methyl (black) protons. No aromatic hydrogen protons are present for 8-bromo-G3 residues.

G-quadruplex also shows a similar result (65). In the case of mode (a), two DMSB molecules and two G-tetrads arrange in interdigitated manner and form two dye-tetrad layers, which should have similar vertical separations. Thus, the distance between two DMSB molecules and that between the G2 and G3 tetrad layer should be close, >6 Å. This distance is much larger than the typical distance of 3.3 Å in a normal cyanine dye dimer (61). In such a distance condition, the exciton transition would be impossible because the intercalation of guanine base between two dye species and thus the characterized D-band (524 nm) in the absorption spectra should not be observed. Thus, mode (a) can be eliminated.

Mode (b) can be excluded by groove block experiment

The quadruplex groove was targeted to determine whether the groove takes part in the dimer/DNA binding. For this purpose, a modified oligonucleotide, ***TG4T-Br***, d(5′-TGG^{Br}GGT-3′), was designed where dG^{Br} is 8-bromo-2′-deoxyguanosine. In the ^{1}H-NMR spectrum of ***TG4T-Br*** (shown in Supporting Information, Supplementary Figure S3), four imino and five aromatic well-defined singlets strongly proved it forms structured parallel-stranded G-quadruplex like ***TG4T***. Compared with ***TG4T***, the Br atom would occupy the center space of each of the four grooves and prevent (or at least limit) the binding of DMSB dimer to the G-quadruplex if the grooves were involved in the interaction.

The ^{1}H-NMR titration experiments of 0.5 mM ***TG4T-Br*** with various concentrations of DMSB were performed, and the original spectra are shown in Supplementary Figure S3 (Supporting Information). The difference in chemical shifts (Δδ) of all the base protons in D-mode stage was calculated and is shown in Figure 5.

Obviously, Δδ values of base protons on ***TG4T-Br*** exhibit a significant decrease compared with those of unmodified ***TG4T*** (Figure 3c). All the Δδ values of ***TG4T-Br*** are as small as <0.05 ppm including G2-NH, indicative of a very weak interaction between DMSB dimer and ***TG4T-Br***. The fact that the blocked groove dramatically weakens the interaction of DMSB dimer with the G-quadruplex suggests the ***TG4T*** groove is involved in the interaction between DMSB and ***TG4T***. As the quadruplex groove plays roles only in mode (c) and mode (d), mode (b) could also be excluded because it is a pure end-stacking mode.

Mode (c) is inconsistent with the results of groove elongation and NOESY experiments

The difference between mode (c) and (d) is the number of sites occupied by DMSB dimer: one for mode (c) (the groove), and two for mode (d) (the groove and the external G2 tetrad). The key point to resolve the two modes is to determine whether the terminal G2-tetrad site participates in the interaction of DMSB with ***TG4T***. To discuss this point in detail, the interactions between DMSB and a series of G-quadruplex samples with different length of grooves, ***TG3T***, ***TG4T***, ***TG6T*** and ***TG8T***, were studied. The formations of intermolecular G-quadruplexes of these sequences were confirmed by CD spectra and polyacrylamide gel electrophoresis experiment (shown in Supporting Information, Supplementary Figure S5, polyacrylamide gel electrophoresis is only for ***TG8T***).

In the pure groove occupation mode like mode (c), cyanine dyes would assemble into linear (helical) aggregates and extend along the groove. It has been reported by Armitage *et al.* (28,66,67) that dimers of cyanine dye Disc$_2$(5), a benzothiazole analog of DMSB, are able to align end–end in the minor groove of a duplex DNA template [Poly-(dA-dT)]$_2$. The AT-5 [d(CGCATATA CGC)/d(GCGTATATGCG)] is able to accommodate one dimer, whereas AT-10 [d(CGCATATATATAT

CGC)/d(GCGATATATATATGCG)] is able to accommodate two end–end adjacent dimers. Similarly, if the DMSB dimers just aligned in the G-quadruplex groove as mode (c) showed, the elongation of the groove length from ***TG3T*** to ***TG6T*** and from ***TG4T*** to ***TG8T*** would be able to accommodate more dye dimers and would result in higher DMSB/DNA binding stoichiometry. However, the UV-vis titration spectra show DMSB in the presence of ***TG3T***, ***TG4T***, ***TG6T*** and ***TG8T*** presents a similar dimer-band profile (shown in Supplementary Figure S6) and similar binding stoichiometry (shown in Figure 6).

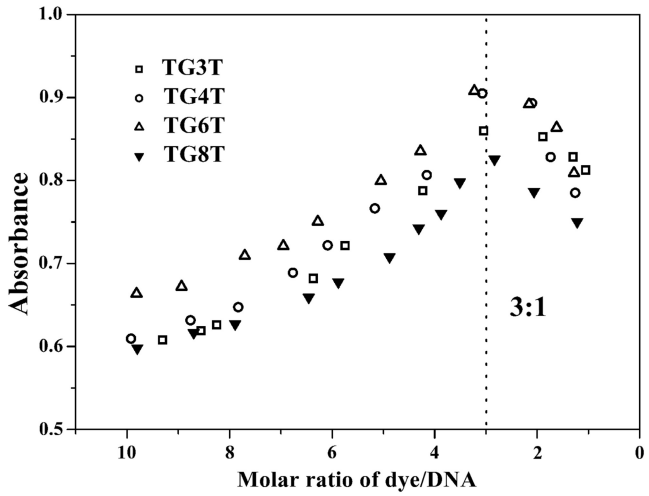

Figure 6. The absorbance variation of the D-band of 12 μM DMSB in the presence of ***TG3T*** (square), ***TG4T*** (circle), ***TG6T*** (hollow triangle) and ***TG8T*** (solid triangle) as a function of the DMSB/G-quadruplex molar ratio.

It seems that the length of the groove does not influence the interaction between DMSB dimer and G-quadruplex.

In addition, CD spectrometer is often used to help explore the binding conformation of small molecules to DNA. As reported in the case of $Disc_2$ (5), end–end adjacent dimers (such as in the duplex minor groove of AT10) could lead to a strong splitting of CD signals of dimer, which results from electronically coupled chromophores between two end–end adjacent dimers (68), whereas individual dimers (such as in AT5) could not. Similarly, in the case of DMSB, the splitting of CD signals of dimer would also be observed if end–end adjacent dimers existed in groove-elongated G-quadruplexes (***TG6T*** or ***TG8T***). However, no such phenomena were found (as shown in Supplementary Figure S7). This result implies that there is no end–end adjacent dimers form and the groove might not be the only key site of DMSB to parallel-stranded G-quadruplex.

Moreover, NOESY spectra also show a definite DMSB insertion between T1 and G2. As shown in Figure 7a, for the unbound ***TG4T***, the G2-H8 shows not only two strong NOE contacts with G2-H2′/H2″ but also two medium NOE contacts with T1-H2′/H2″, indicating spatially close G2 and T1. However, in the presence of DMSB, as shown in Figure 7b, the NOE contacts between G2-H8 and T1-H2′/H2″ disappear and only the two G2-H8:G2-H2′/H2″ NOE signals remain. This strongly demonstrates the insertion of DMSB into the binding cavity between G2 and T1, which shows evidence of T1 moving away from G2. Accompanying the significant great chemical shift of G2-NH shown in Figure 3c, this result further proves partial dimer inserts into the space between terminal G2 tetrad and T1 when it binds to ***TG4T*** near 5′-end.

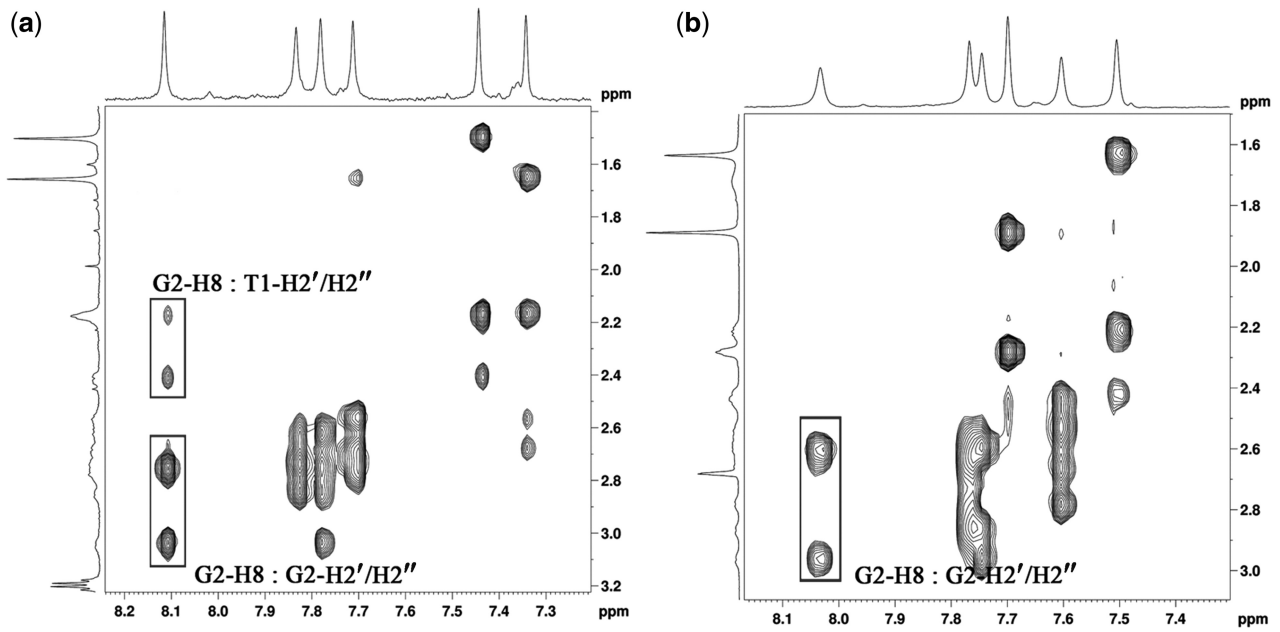

Figure 7. The partial expanded region of NOESY spectra for 0.5 mM (2 mM single-strand concentration) unbound ***TG4T*** (**a**) and 5:1 DMSB–***TG4T*** complex (**b**) (600 MHz, 308 K) in 0.4 mL phosphate buffer containing 20 mM KH_2PO_4/K_2HPO_4, 70 mM KCl, PH 7.4 (H_2O/D_2O 9:1, v/v).

In a word, both the absorption and CD results indicate the elongation of G-quadruplex groove does not facilitate the end–end alignment of DMSB dimer in the groove. The NOESY result further demonstrates directly the involvement of external G-tetrad. These facts do not support mode (c).

Because modes (a), (b) and (c) in Figure 4 are inconsistent with the theoretical or experimental results, mode (d), the dual-site simultaneous binding mode, might be the most possible mode between DMSB and ***TG4T*** in D-mode stage. In other words, both the groove and the terminal G-tetrad at 5′-end play critical roles in the interaction.

Ligand displacement result supports the dual-site simultaneous binding mode

If DMSB dimer occupies the groove and G-tetrad simultaneously, it is reasonable to deduce that addition of any other end-stacking binder or groove binder will weaken the DMSB dimer binding for competitive reason. Studies demonstrate that methylene blue (MB) is an end-stacking quadruplex binder (69,70), whereas the 3,6-Bis-(1-methyl-4-vinylpyridium iodine) 9-ethyl-carbazole (BMVEC) is a groove binder when the BMVEC:quadruplex stoichiometry is <2:1 (24). Here we use the two ligands to carry out the ligand displacement studies to further confirm the dual-site binding mode. As shown in Supplementary Figure S8a, addition of 1–2 μM MB causes fluorescence intensity decrease of both bound monomer and bound dimer of DMSB, indicating both 3′ and 5′ external tetrad occupied by MB. The result is consistent with the fact that DMSB monomer binds to 3′-end, whereas the DMSB dimer binds to 5′-end. When 1–2 μM BMVEC is added, it apparently appears that only the fluorescence intensity of DMSB dimer is weakened, indicating the groove binder BMVEC only influences the dimer binding of DMSB. The ligand displacement result provides an indirect evidence for the dual-site simultaneous binding mode.

NOESY spectrum gives direct evidences about the dual-site simultaneous binding mode

The NOESY spectrum could provide direct evidences to further support the binding mode. The key NOE contacts associated with the dual-site binding mode were tabulated in Table 1 and pointed out in Supplementary Figure S9. Firstly, the clear dye–dye intermolecular NOE contacts between meso-methyl proton H8 and the four aromatic ring protons H1, H2, H3 and H4 undoubtedly reveal the presence of DMSB dimer (Supplementary Figure S9a). Secondly, the DMSB meso-methyl proton H8 shows medium NOE contacts with both G2-H8 (Supplementary Figure S9a) and G2-NH (Supplementary Figure S9d), indicative of DMSB dimers locating near the G2 base. The aromatic protons H1, H2 and H3 show medium NOE contacts with G2-NH but without any contacts with G3-NH (Supplementary Figure S9c), which implies the aromatic ring of DMSB locates at the external G2 tetrad. Thirdly, aromatic protons H1 and H2 on DMSB show two relatively weak NOE signals with G3-H8 but without any NOE contacts with G4-H8 (Supplementary Figure S9b), indicating that the DMSB aromatic ring inserts into the groove and is farther from G4-H8 than G3-H8. All these NOESY results suggest that the DMSB dimer occupies both the external G2 tetrad and the corresponding groove of ***TG4T***, which is a dual-site simultaneous binding.

Table 1. The key intermolecular NOESY contacts for dye-dye and dye-DNA in D-mode

Interaction	NOE signals			NOESY spectrum
	Protons		Strength	
	DMSB	*TG4T*		
dye-dye contacts inside DMSB dimer	H8-H1 H8-H2 H8-H3 H8-H4		Medium	Figure S9a
dye-DNA contacts between DMSB and the external G2-tetrad of ***TG4T***	H8 H8 H1 H2 H3	G2-H8 G2-NH G2-NH G2-NH G2-NH	Medium	Figure S9a Figure S9d Figure S9c
dye-DNA contacts between DMSB and the groove of ***TG4T***	H1 H2	G3-H8 G3-H8	Weak	Figure S9b

Docking study of DMSB–TG4T complex

Molecular dynamics simulation of the complex

To get a clearer image of the interaction, the structure of DMSB–***TG4T*** complex was calculated by using dynamics simulation in Discovery Studio based on NOE constraints extracted from 5:1 DMSB/***TG4T*** NOESY spectrum. The full resonance signal assignments for ***TG4T*** and DMSB in the complex were tabulated in Supplementary Tables S1 and S2, respectively. The original NOESY spectrum was presented in Supplementary Figure S9. TOCSY spectrum used for assisting resonance assignment was shown in Supplementary Figure S10. The NOE constraints, derived from DNA–DNA, dye–DNA and dye–dye contacts, were extracted from FELIX program and used in molecular dynamics simulation, which are profiled in Supplementary Table S3. For more details, the dye–DNA and dye–dye contacts found in NOESY spectrum were listed in Supplementary Table S4. In 500 ps dynamic simulation, the ensemble equilibrium is achieved at ~150 ps, which can be reflected by system temperature, and especially by the potential energy (shown in Supplementary Figure S11). Ten best conformations were extracted from the last 50 ps simulation trajectories, which had the lowest potential energy and superimposed together, as shown in Figure 8a. A surface model, which profiles the surface electrostatic potential, is also given in Figure 8b.

The dynamics simulation results are in accordance with the aforementioned conclusions based on experiments. For the monomer binding stage, one DMSB stacks above G5 tetrad, with two T6 residues covered to stabilize the stacking conformation (Supplementary Figure S8a).

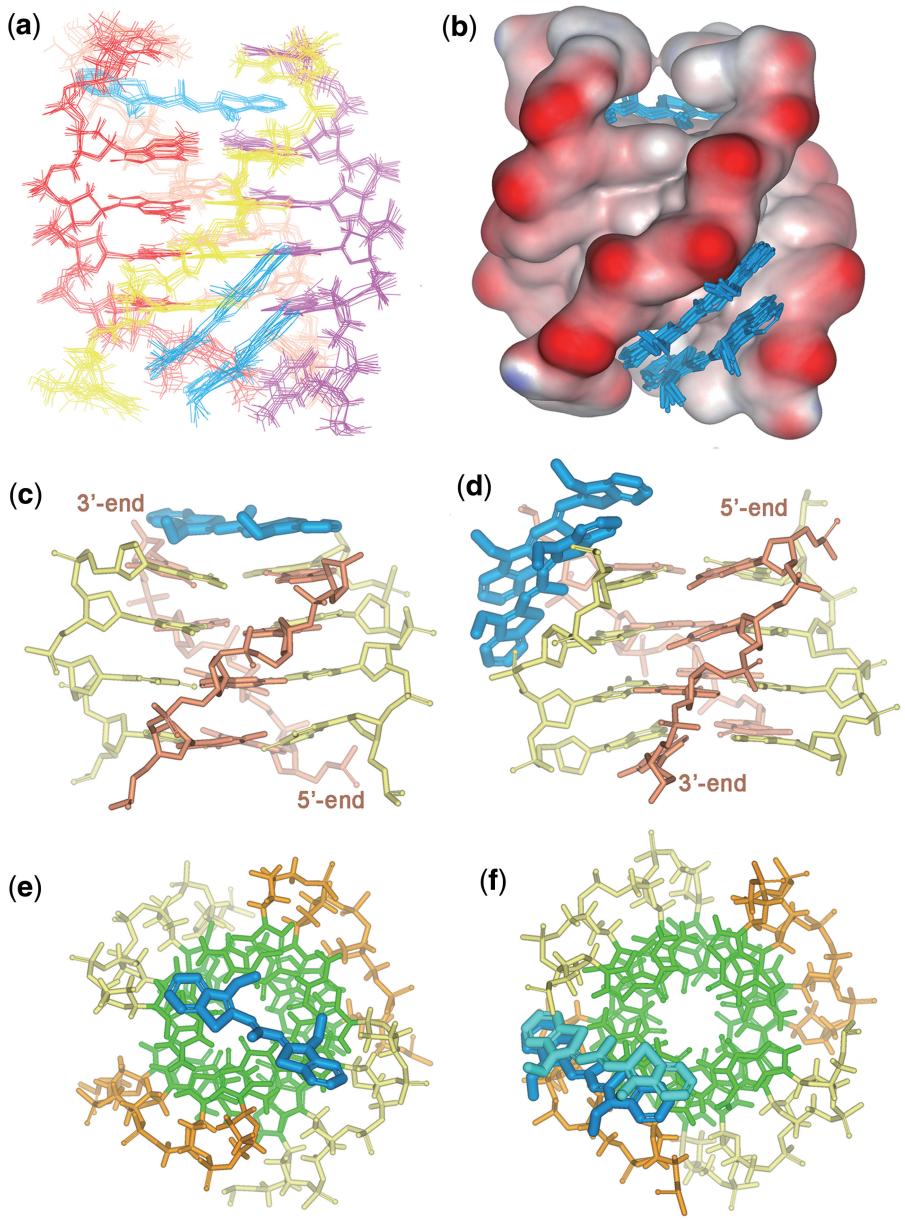

Figure 8. (**a**) The superimposition of the 10 best DMSB/***TG4T*** complex structures taken from the last 50 ps of the NOE-restrained dynamics simulation where the DMSB molecules are light blue. (**b**) The Delphi electrostatic potential surface view of the 10 best complex structures superimposition, where negative charge is colored by red, positive charge by blue and neutral by white. The side view (**c**) and top view (**e**) of monomer binding site at 3′-end, and side view (**d**) and top view (**f**) of dimer binding site at 5′-end where DMSB is colored light blue. The thymine bases on both end were removed to get a clear view.

The DMSB molecule exhibits a slight torsion rather than a complete planar to match with a thymine ring (Figure 8c and e). Weak negative CD signals at M-band (~554 nm) of DMSB induced by ***TG4T*** (shown in Supplementary Figure S7) are in accordance with this weak asymmetric distortion of the chromophore of DMSB.

For the dimer binding stage, two DMSB molecules form an indented arranged H-dimer and bind on the 5′-end of ***TG4T***, as shown in Figure 8d and f. The dimer binding spans two sites of the G-quadruplex, with one benzoselenazole unit stacking on the G2 tetrad partially and the other inserting into the groove, pointing to the 3′-end of ***TG4T***.

DMSB dimer is relatively rigid and not embedded into the groove of TG4T completely

An interesting point is that the simulation result shows the aromatic ring of DMSB is not embedded into the groove of ***TG4T*** completely in the D-mode stage, which could be seen clearly in Figure 8d. This result is in accordance with the relatively weak NOE signals between DMSB aromatic protons and G3-H8. There is no significant difference between CD signals of unbound DMSB dimers and those of bound ones (Supplementary Figure S7, 527 nm), implying that DMSB molecules in the dimer are relatively rigid and their conformation alterations are very weak. This might be the reason of the incomplete

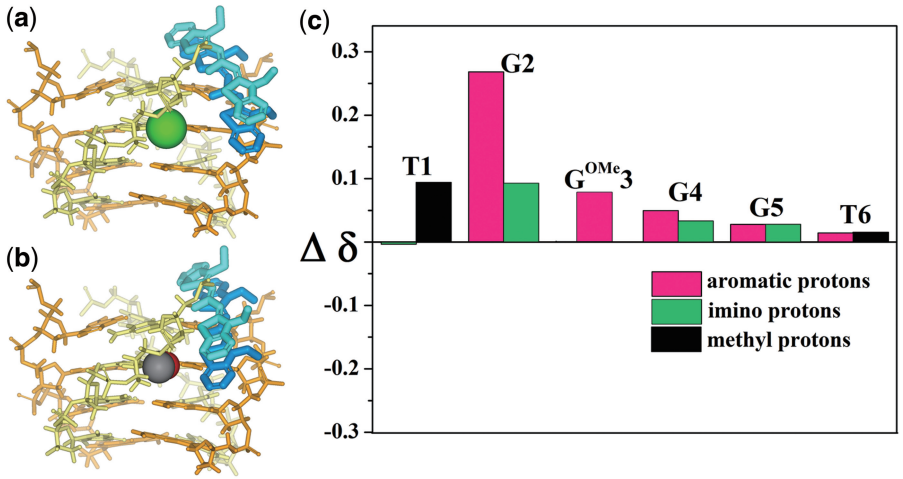

Figure 9. Schematic presentation of (**a**) Br and (**b**) methoxyl substituted ***TG4T*** when binding to DMSB dimer. (**c**) Changes in chemical shifts (Δδ) of base protons on ***TG4T-OMe*** with DMSB in D-mode stage (chemical shifts of 1:8 ***TG4T-OMe***/DMSB complex to those of 1:3 ***TG4T-OMe***/DMSB complex). Δδ values are reported for aromatic (magenta), imino (green) and methyl (black) protons. No aromatic hydrogen protons are present for modified G3 residues.

insertion of aromatic rings of DMSB dimer into the groove.

To further validate the fact of incomplete embedding, another modified G-quadruplex sample ***TG4T-OMe***, $[d(5'\text{-}TGG^{OMe}GGT\text{-}3')]_4$, where dG^{OMe} is 8-methoxy-2′-deoxyguanosine, was synthesized (the formation of G-quadruplex structures have been confirmed by ^{1}H-NMR spectra, shown in Supporting Information, Supplementary Figure S4). Similar to ***TG4T-Br***, ***TG4T-OMe*** also could provide a groove-blocked G-quadruplex model. The difference is that the size of Br is larger (the covalent radius of Br is 114 pm) than that of methoxyl group (the covalent radius of C and O is 77 and 73 pm, respectively). Besides, methoxyl group is flexible and can rotate and alter its orientation to avoid unfavorable collisions. So Br occupies larger groove space and possesses stronger groove block effect than methoxyl group does (shown in Figure 9a and b). Changes in chemical shifts (Δδ) of base protons on ***TG4T-OMe*** with DMSB during D-mode stage are summarized in Figure 9c (the original ^{1}H-NMR spectra are shown in Supplementary Figure S4). Comparing Figure 9c with Figure 6 and Figure 3c, we could see that ***TG4T-OMe*** presents similar Δδ values to ***TG4T*** but much stronger Δδ values than that of ***TG4T-Br***. The fact that the larger blocker Br can hinder the binding of DMSB dimer to G-quadruplex while the smaller methoxyl group cannot is well consistent with the dimer-binding mode revealed by dynamic simulation, which shows the incomplete embedding of DMSB dimer in the G-quadruplex groove.

Non-bond interaction energy analysis for the two binding modes

The interaction energies for DNA-monomer and DNA-dimer were calculated by using the Interaction Energy Calculation protocol. The summation of Van der Waals and electrostatic interaction energy is shown in Table 2. Note that the total non-bond interaction energy for DNA-monomer (-11.25 kcal·mol^{-1}) is lower than that for DNA-dimer (-8.86 kcal·mol^{-1}), implying a stronger binding affinity for DMSB monomer than for dimer. This result is well complied with the fact that DMSB preferentially binds to ***TG4T*** in the form of monomer when DMSB is insufficient. Furthermore, the Van der Waals energy term is close to electrostatic energy term, suggesting the contributions of hydrophobic effect and electrostatic force in the binding are similar.

Table 2. The nonbond interaction energy between ***TG4T*** and DMSB

Energy terms	DNA-monomer interaction (kcal·mol^{-1})	DNA-dimer interaction (kcal·mol^{-1})
Van der Waals energy	−6.80	−4.80
Electrostatic energy	−4.45	−4.06
Total nonbond energy	−11.25	−8.86

Discussion on structural features of DMSB with the dual-site binding mode

In this article, after replacement of the naphthothiazole scaffold of ETC (13) by the benzoselenazole unit, as well as the removal of cationic sulfo group from the *N*-alkyl chains, DMSB unexpectedly adopts a dual-site simultaneous binding mode with ***TG4T***. It is inferred that a shortened and non-polar *N*-alkyl chain may be a key factor to this binding mode. Distamycin-A, which is another case (also the only case) of ligand binding on G-quadruplex in the dual-site mode, indicates a similar conclusion. Randazzo and colleagues (27) reported that distamycin-A, which has a cationic amidinium, adopts a pure groove binding mode on ***TG4T***. While after a positively charged amidinium moiety was replaced by an uncharged *N*-methyl amide, distamycin-A derivative occupies both the groove and the 3′-end of ***TG4T***. The aforementioned works give us a clue that although

cationic group could enhance the interaction to G-quadruplex via attracting its anionic phosphate-backbone, non-polar group might facilitate a dual-site binding mode, which could provide a new idea in further designing of highly specific G-quadruplex probes.

DMSB dimer shows specific recognition ability to parallel G-quadruplex

To clarify the roles of the dual-site simultaneous binding mode in G-quadruplex recognition, the specificities of DMSB and ETC (an excellent G-quadruplex probe we previously reported) against 11 DNAs with various motifs (details in Supplementary Table S5) are compared. As shown in Supplementary Figure S12, it indicates that both the two probes are able to well distinguish G-quadruplex from duplex and single-strand DNA, but they present different recognition abilities among G-quadruplexes. Depending on the end-stacking recognizing mode, ETC could respond to G-quadruplex motifs with exposed terminal G-tetrad, such as intramolecular parallel-stranded (***c-myc 2345*** and ***c-kit1***) and mixed-type (***M24***) G-quadruplex, as well as antiparallel-stranded G-quadruplex without diagonal loop (***TBA***), but is negative to ***TG_4T*** and ***H7***, which are intermolecular parallel-stranded G-quadruplex with covered terminal G-tetrad. On the other hand, DMSB, characterized by the dual-site simultaneous binding, could discriminate parallel-stranded G-quadruplex from the other studied motifs including both mixed-type and antiparallel G-quadruplexes. In this sense, DMSB seems to exhibit higher specificity than ETC, implying the potential enhancement ability for probe specificity by the dual-site mode.

Furthermore, the binding affinities of DMSB dimer to various DNA motifs were also evaluated by the melting experiments. From the dimer point of view, as shown in Supplementary Table S6 and Supplementary Figure S13a, the melting temperature (Tm) of bound dimers exceeds 95°C due to binding to ***TG4T*** compared with that of free dimers, which is ~35°C, regardless of the absence or presence of other DNA motifs (including the antiparallel-stranded ***H22*** and the duplex ***CT***). Apparently, the stability of dimers is greatly enhanced for the binding to parallel quadruplex ***TG4T***. From the DNA point of view, as shown in Supplementary Table S6 and Supplementary Figure S13b, only the stability of parallel-stranded G-quadruplex ***c-myc 2345*** is greatly enhanced by DMSB with a Tm increase of >30°C. The contribution of DMSB to Tm of antiparallel-stranded ***H22*** and duplex ***CT*** is much less than that of ***c-myc 2345*** (~3°C and 2°C, respectively). It could also be found that even in the presence of large amount of ***CT***, DMSB dimer could stabilize ***c-myc 2345*** well. In addition, the tendency of melting curves of bound dimers in Supplementary Figure S13a is similar to that of ***c-myc 2345*** in Supplementary Figure S13b, indicating that the binding makes the dimer and parallel G-quadruplex stabilize each other. These results imply relatively nice binding affinity and selectivity of DMSB dimers against parallel-stranded G-quadruplexes.

CONCLUSION

We revealed in this article that the cyanine dye DMSB is capable of binding to a parallel-stranded quadruplex ***TG4T*** in the form of monomer and dimer in different sites. The dimer binding is a dual-site simultaneous binding mode, which is different from normal modes (such as end-stacking or pure groove-embedding). This kind of binding mode involves two unique structural features of G-quadruplex, terminal G-tetrad and groove, which might help improve the specificity of the ligands.

The detailed mechanism discussion demonstrates that DMSB monomers can stack on the terminal G-tetrad at 3′-end in lower [DMSB]/[***TG4T***] ratio, whereas DMSB dimers bind to ***TG4T*** by occupying both the 5′-end external G-tetrad and the corresponding groove in higher [DMSB]/[***TG4T***] ratio, namely, the dual-site simultaneous binding mode. These findings as well as the structural elucidation might provide clues in aspects of designing highly specific G-quadruplex probes.

SUPPLEMENTARY DATA

Supplementary Data are available at NAR Online: Supplementary Tables 1–6, Supplementary Figures 1–13 and Supplementary References [71–77].

ACKNOWLEDGEMENTS

The authors greatly thank Professor Randazzo Antonio and Professor Janice Aldrich-Wright for their valuable suggestions to our work.

FUNDING

Funding for open access charge: National Natural Science Foundation of China [91027033, 81072576, 21205121 and 31200576]; the Chinese Academy of Sciences [KJCX2-EW-N06-01].

Conflict of interest statement. None declared.

REFERENCES

1. Hurley,L.H., Siddiqui-Jain,A., Grand,C.L. and Bearss,D.J. (2002) Direct evidence for a G-quadruplex in a promoter region and its targeting with a small molecule to repress c-MYC transcription. *Proc. Natl Acad. Sci. USA*, **99**, 11593–11598.
2. Sun,D.Y., Thompson,B., Cathers,B.E., Salazar,M., Kerwin,S.M., Trent,J.O., Jenkins,T.C., Neidle,S. and Hurley,L.H. (1997) Inhibition of human telomerase by a G-quadruplex-interactive compound. *J. Med. Chem.*, **40**, 2113–2116.
3. Neidle,S., Burge,S., Parkinson,G.N., Hazel,P. and Todd,A.K. (2006) Quadruplex DNA: sequence, topology and structure. *Nucleic Acids Res.*, **34**, 5402–5415.
4. Williamson,J.R. (1994) G-quartet structures in telomeric DNA. *Annu. Rev. Biophys. Biomol. Struct.*, **23**, 703–730.
5. Williamson,J.R., Raghuraman,M.K. and Cech,T.R. (1989) Monovalent cation-induced structure of telomeric DNA: the G-quartet model. *Cell*, **59**, 871–880.
6. Huppert,J.L. and Balasubramanian,S. (2007) G-quadruplexes in promoters throughout the human genome. *Nucleic Acids Res.*, **35**, 406–413.
7. Wang,Y. and Patel,D.J. (1992) Guanine Residues in D(T2ag3) and D(T2g4) form parallel-stranded potassium cation stabilized

g-quadruplexes with antiglycosidic torsion angles in solution. *Biochemistry*, **31**, 8112–8119.
8. Izbicka,E., Nishioka,D., Marcell,V., Raymond,E., Davidson,K.K., Lawrence,R.A., Wheelhouse,R.T., Hurley,L.H., Wu,R.S. and Von Hoff,D.D. (1999) Telomere-interactive agents affect proliferation rates and induce chromosomal destabilization in sea urchin embryos. *Anticancer Drug Des.*, **14**, 355–365.
9. Tauchi,T., Shin-Ya,K., Sashida,G., Sumi,M., Nakajima,A., Shimamoto,T., Ohyashiki,J.H. and Ohyashiki,K. (2003) Activity of a novel G-quadruplex-interactive telomerase inhibitor, telomestatin (SOT-095), against human leukemia cells: involvement of ATM-dependent DNA damage response pathways. *Oncogene*, **22**, 5338–5347.
10. Cocco,M.J., Hanakahi,L.A., Huber,M.D. and Maizels,N. (2003) Specific interactions of distamycin with G-quadruplex DNA. *Nucleic Acids Res.*, **31**, 2944–2951.
11. Izbicka,E., Wheelhouse,R.T., Raymond,E., Davidson,K.K., Lawrence,R.A., Sun,D.Y., Windle,B.E., Hurley,L.H. and Von Hoff,D.D. (1999) Effects of cationic porphyrins as G-quadruplex interactive agents in human tumor cells. *Cancer Res.*, **59**, 639–644.
12. Chang,T.C. and Chang,C.C. (2010) Detection of G-quadruplexes in cells and investigation of G-quadruplex structure of d(T(2)AG(3))(4) in K+ solution by a carbazole derivative: BMVC. *Methods Mol. Biol.*, **608**, 183–206.
13. Yang,Q.F., Xiang,J.F., Yang,S., Li,Q., Zhou,Q.J., Guan,A.J., Zhang,X.F., Zhang,H., Tang,Y.L. and Xu,G.Z. (2010) Verification of specific G-quadruplex structure by using a novel cyanine dye supramolecular assembly: part II. The binding characterization with specific intramolecular G-quadruplex and the recognizing mechanism. *Nucleic Acids Res.*, **38**, 1022–1033.
14. Mita,H., Ohyama,T., Tanaka,Y. and Yamamoto,Y. (2006) Formation of a complex of 5,10,15,20-tetrakis(N-methylpyridinium-4-yl)-21H,23H-porphyrin with G-quadruplex DNA. *Biochemistry*, **45**, 6765–6772.
15. Han,F.X.G., Wheelhouse,R.T. and Hurley,L.H. (1999) Interactions of TMPyP4 and TMPyP2 with quadruplex DNA. Structural basis for the differential effects on telomerase inhibition. *J. Am. Chem. Soc.*, **121**, 3561–3570.
16. Kim,M.Y., Vankayalapati,H., Kazuo,S., Wierzba,K. and Hurley,L.H. (2002) Telomestatin, a potent telomerase inhibitor that interacts quite specifically with the human telomeric intramolecular G-quadruplex. *J. Am. Chem. Soc.*, **124**, 2098–2099.
17. Li,Z., Tan,J.-H., He,J.-H., Long,Y., Ou,T.-M., Li,D., Gu,L.-Q. and Huang,Z.-S. (2012) Disubstituted quinazoline derivatives as a new type of highly selective ligands for telomeric G-quadruplex DNA. *Eur. J. Med. Chem.*, **47**, 299–311.
18. Pilch,D.S., Barbieri,C.M., Rzuczek,S.G., LaVoie,E.J. and Rice,J.E. (2008) Targeting human telomeric G-quadruplex DNA with oxazole-containing macrocyclic compounds. *Biochimie*, **90**, 1233–1249.
19. Sun,H.X., Tang,Y.L., Xiang,J.F., Xu,G.Z., Zhang,Y.Z., Zhang,H. and Xu,L.H. (2006) Spectroscopic studies of the interaction between quercetin and G-quadruplex DNA. *Bioorg. Med. Chem. Lett.*, **16**, 3586–3589.
20. Randazzo,A., Galeone,A. and Mayol,L. (2001) H-1-NMR study of the interaction of distamycin A and netropsin with the parallel stranded tetraplex $[d(TGGGGT)]_4$. *Chem. Commun.*, **11**, 1030–1031.
21. Martino,L., Virno,A., Pagano,B., Virgilio,A., Di Micco,S., Galeone,A., Giancola,C., Bifulco,G., Mayol,L. and Randazzo,A. (2007) Structural and thermodynamic studies of the interaction of distamycin A with the parallel quadruplex structure $[d(TGGGGT)]_4$. *J. Am. Chem. Soc.*, **129**, 16048–16056.
22. Dash,J., Shirude,P.S., Hsu,S.T.D. and Balasubramanian,S. (2008) Diarylethynyl Amides that recognize the parallel conformation of genomic promoter DNA G-quadruplexes. *J. Am. Chem. Soc.*, **130**, 15950–15956.
23. Chang,C.-C., Chien,C.-W., Lin,Y.-H., Kang,C.-C. and Chang,T.-C. (2007) Investigation of spectral conversion of d(TTAGGG)4 and d(TTAGGG)13 upon potassium titration by a G-quadruplex recognizer BMVC molecule. *Nucleic Acids Res.*, **35**, 2846–2860.
24. Zhang,X.F., Zhang,H.J., Xiang,J.F., Li,Q.A., Yang,Q.F., Shang,Q.A., Zhang,Y.X. and Tang,Y.L. (2010) The binding modes of carbazole derivatives with telomere G-quadruplex. *J. Mol. Struct.*, **982**, 133–138.
25. Patel,D.J., Phan,A.T. and Kuryavyi,V. (2007) Human telomere, oncogenic promoter and 5'-UTR G-quadruplexes: diverse higher order DNA and RNA targets for cancer therapeutics. *Nucleic Acids Res.*, **35**, 7429–7455.
26. Cosconati,S., Marinelli,L., Trotta,R., Virno,A., Mayol,L., Novellino,E., Olson,A.J. and Randazzo,A. (2009) Tandem application of virtual screening and NMR experiments in the discovery of brand new DNA quadruplex groove binders. *J. Am. Chem. Soc.*, **131**, 16336–16337.
27. Cosconati,S., Marinelli,L., Trotta,R., Virno,A., De Tito,S., Romagnoli,R., Pagano,B., Limongelli,V., Giancola,C., Baraldi,P.G. *et al.* (2010) Structural and conformational requisites in DNA quadruplex groove binding: another piece to the puzzle. *J. Am. Chem. Soc.*, **132**, 6425–6433.
28. Wang,M.M., Silva,G.L. and Armitage,B.A. (2000) DNA-templated formation of a helical cyanine dye J-aggregate. *J. Am. Chem. Soc.*, **122**, 9977–9986.
29. Zhang,Y., Xiang,J., Tang,Y., Xu,G. and Yan,W. (2007) Chiral transformation of achiral J-aggregates of a cyanine dye templated by human serum albumin. *Chemphyschem*, **8**, 224–226.
30. Yang,Q., Xiang,J., Yang,S., Zhou,Q., Li,Q., Tang,Y. and Xu,G. (2009) Verification of specific G-quadruplex structure by using a novel cyanine dye supramolecular assembly: part I. Recognizing mixed G-quadruplex in human telomeres. *Chem. Commun.*, 1103–1105.
31. Brooker,L.G.S. and White,F.L. (1935) Studies in the cyanine dye series: part I. A new method of preparing certain carbocyanines. *J. Am. Chem. Soc.*, **57**, 547–551.
32. Hamer,F.M. (1964) *The Cyanine Dyes and Related Compounds*. Interscience Publishers, New York.
33. Piotto,M., Saudek,V. and Sklenar,V. (1992) Gradient-tailored excitation for single-quantum NMR spectroscopy of aqueous solutions. *J. Biomol. NMR*, **2**, 661–665.
34. Sklenar,V., Piotto,M., Leppik,R. and Saudek,V. (1993) Gradient-tailored water suppression for H-1-N-15 Hsqc experiments optimized to retain full sensitivity. *J. Magn. Reson. Ser. A*, **102**, 241–245.
35. Jeener,J., Meier,B.H., Bachmann,P. and Ernst,R.R. (1979) Investigation of exchange processes by 2-dimensional NMR-spectroscopy. *J. Chem. Phys.*, **71**, 4546–4553.
36. Marion,D., Ikura,M., Tschudin,R. and Bax,A. (1989) Rapid recording of 2d NMR-spectra without phase cycling - application to the study of hydrogen-exchange in proteins. *J. Magn. Reson.*, **85**, 393–399.
37. Jorgensen,W.L. (1982) Quantum and Statistical mechanical studies of liquids .24. Revised tips for simulations of liquid water and aqueous-solutions. *J. Chem. Phys.*, **77**, 4156–4163.
38. Allen,M.P. and Tildesley,D.J. (1987) *Computer Simulation of Liquids*. Oxford University Press, Oxford, UK.
39. Berendsen,H.J.C., Postma,J.P.M., Vangunsteren,W.F., Dinola,A. and Haak,J.R. (1984) Molecular-dynamics with coupling to an external bath. *J. Chem. Phys.*, **81**, 3684–3690.
40. Nose,S. (1984) A molecular-dynamics method for simulations in the canonical ensemble. *Mol. Phys.*, **52**, 255–268.
41. Hoover,W.G. (1985) Canonical dynamics - equilibrium phase-space distributions. *Phys. Rev. A.*, **31**, 1695–1697.
42. Darden,T., York,D. and Pedersen,L. (1993) Particle mesh ewald - an N.Log(N) method for ewald sums in large systems. *J. Chem. Phys.*, **98**, 10089–10092.
43. Ryckaert,J.P., Ciccotti,G. and Berendsen,H.J.C. (1977) Numerical-integration of cartesian equations of motion of a system with constraints - molecular-dynamics of N-alkanes. *J. Comput. Phys.*, **23**, 327–341.
44. Hockney,R.W. (1970) *The Potential Calculation and Some Applications*. Academic Press, New York.
45. Mishra,A., Behera,R.K., Behera,P.K., Mishra,B.K. and Behera,G.B. (2000) Cyanines during the 1990s: a Review. *Chem. Rev.*, **100**, 1973–2012.
46. Chibisov,A.K., Zakharova,G.V. and Gorner,H. (1999) Photoprocesses in dimers of thiacarbocyanines. *Phys. Chem. Chem. Phys.*, **1**, 1455–1460.
47. Herz,A.H. (1974) Dye-dye interactions of cyanines in solution and at AgBr surfaces. *Photogr. Sci. Eng.*, **18**, 323–335.

48. Herz,A.H. (1977) Aggregation of sensitizing dyes in solution and their adsorption onto silver halides. *Adv. Colloid Interface Sci.*, **8**, 237–298.
49. West,W. and Pearce,S. (1965) Dimeric state of cyanine dyes. *J. Phys. Chem.*, **69**, 1894–1903.
50. McRae,E.G. and Kasha,M. (1958) Enhancement of phosphoescence ability upon aggregation of dye molecules. *J. Chem. Phys.*, **28**, 721–722.
51. Chibisov,A.K. and Gorner,H. (2002) Photophysics of aggregated 9-methylthiacarbocyanine bound to polyanions. *Chem. Phys. Lett.*, **357**, 434–439.
52. McPhee,J.T., Scott,E., Levinger,N.E. and Van Orden,A. (2011) Cy3 in AOT reverse micelles II. Probing intermicellar interactions using fluorescence correlation spectroscopy. *J. Phys. Chem. B*, **115**, 9585–9592.
53. Aboul-ela,F., Murchie,A.I. and Lilley,D.M. (1992) NMR study of parallel-stranded tetraplex formation by the hexadeoxynucleotide d(TG4T). *Nature*, **360**, 280–282.
54. Phan,A.T., Modi,Y.S. and Patel,D.J. (2004) Propeller-type parallel-stranded g-quadruplexes in the human c-myc promoter. *J. Am. Chem. Soc.*, **126**, 8710–8716.
55. Phan,A.T., Kuryavyi,V., Burge,S., Neidle,S. and Patel,D.J. (2007) Structure of an unprecedented G-quadruplex scaffold in the human c-kit promoter. *J. Am. Chem. Soc.*, **129**, 4386–4392.
56. Parkinson,G.N., Lee,M.P.H. and Neidle,S. (2002) Crystal structure of parallel quadruplexes from human telomeric DNA. *Nature*, **417**, 876–880.
57. Aboul-ela,F., Murchie,A.I., Norman,D.G. and Lilley,D.M. (1994) Solution structure of a parallel-stranded tetraplex formed by d(TG4T) in the presence of sodium ions by nuclear magnetic resonance spectroscopy. *J. Mol. Biol.*, **243**, 458–471.
58. Laughlan,G., Murchie,A.I., Norman,D.G., Moore,M.H., Moody,P.C., Lilley,D.M. and Luisi,B. (1994) The high-resolution crystal structure of a parallel-stranded guanine tetraplex. *Science*, **265**, 520–524.
59. Tatikolov,A.S. and Costa,S.M. (2004) Complexation of polymethine dyes with human serum albumin: a spectroscopic study. *Biophys. Chem.*, **107**, 33–49.
60. McPhee,J.T., Scott,E., Levinger,N.E. and Van Orden,A. (2011) Cy3 in AOT reverse micelles I. Dimer formation revealed through steady-state and time-resolved spectroscopy. *J. Phys. Chem. B*, **115**, 9576–9584.
61. Rosch,U., Yao,S., Wortmann,R. and Wurthner,F. (2006) Fluorescent H-aggregates of merocyanine dyes. *Angew. Chem. Int. Ed.*, **45**, 7026–7030.
62. Bergmann,K. and Okonski,C.T. (1963) A spectroscopic study of methylene blue monomer, dimer, and complexes with montmorillonite. *J. Phys. Chem.*, **67**, 2169–2177.
63. Watson,J.D. and Crick,F.H. (1953) Molecular structure of nucleic acids; a structure for deoxyribose nucleic acid. *Nature*, **171**, 737–738.
64. Benevides,J.M. and Thomas,G.J. (2005) Local conformational changes induced in B-DNA by ethidium intercalation. *Biochemistry*, **44**, 2993–2999.
65. Wei,C., Jia,G., Yuan,J., Feng,Z. and Li,C. (2006) A spectroscopic study on the interactions of porphyrin with G-quadruplex DNAs. *Biochemistry*, **45**, 6681–6691.
66. Seifert,J.L., Connor,R.E., Kushon,S.A., Wang,M. and Armitage,B.A. (1999) Spontaneous assembly of helical cyanine dye aggregates on DNA nanotemplates. *J. Am. Chem. Soc.*, **121**, 2987–2995.
67. Armitage,B.A. (2005) Cyanine dye-DNA interactions: intercalation, groove binding, and aggregation. *Top. Curr. Chem.*, **253**, 55–76.
68. Gargiulo,D., Ikemoto,N., Odingo,J., Bozhkova,N., Iwashita,T., Berova,N. and Nakanishi,K. (1994) CD Exciton chirality method - Schiff-base and cyanine dye-type chromophores for primary amino-groups. *J. Am. Chem. Soc.*, **116**, 3760–3767.
69. Chan,D.S.H., Yang,H., Kwan,M.H.T., Cheng,Z., Lee,P., Bai,L.P., Jiang,Z.H., Wong,C.Y., Fong,W.F., Leung,C.H. *et al.* (2011) Structure-based optimization of FDA-approved drug methylene blue as a c-myc G-quadruplex DNA stabilizer. *Biochimie*, **93**, 1055–1064.
70. Sun,H.X., Xiang,J.F., Zhang,Y.Z., Xu,G.Z., Xu,L.H. and Tang,Y.L. (2006) Spectroscopic studies of the interaction between methylene blue and G-quadruplex. *Chin. Sci. Bull.*, **51**, 1687–1692.
71. Bock,L.C., Griffin,L.C., Latham,J.A., Vermaas,E.H. and Toole,J.J. (1992) Selection of single-stranded-DNA molecules that bind and inhibit human thrombin. *Nature*, **355**, 564–566.
72. Wang,Y. and Patel,D.J. (1993) Solution structure of the human telomeric repeat d[AG3(T2AG3)3] G-tetraplex. *Structure*, **1**, 263–282.
73. Granotier,C., Pennarun,G., Riou,L., Hoffschir,F., Gauthier,L.R., De Cian,A., Gomez,D., Mandine,E., Riou,J.F., Mergny,J.L. *et al.* (2005) Preferential binding of a G-quadruplex ligand to human chromosome ends. *Nucleic Acids Res.*, **33**, 4182–4190.
74. Rujan,I.N., Meleney,J.C. and Bolton,P.H. (2005) Vertebrate telomere repeat DNAs favor external loop propeller quadruplex structures in the presence of high concentrations of potassium. *Nucleic Acids Res.*, **33**, 2022–2031.
75. Li,J., Correia,J.J., Wang,L., Trent,J.O. and Chaires,J.B. (2005) Not so crystal clear: the structure of the human telomere G-quadruplex in solution differs from that present in a crystal. *Nucleic Acids Res.*, **33**, 4649–4659.
76. Phan,A.T., Luu,K.N. and Patel,D.J. (2006) Different loop arrangements of intramolecular human telomeric (3+1) G-quadruplexes in K+ solution. *Nucleic Acids Res.*, **34**, 5715–5719.
77. Amrane,S., Ang,R.W., Tan,Z.M., Li,C., Lim,J.K., Lim,J.M., Lim,K.W. and Phan,A.T. (2009) A novel chair-type G-quadruplex formed by a Bombyx mori telomeric sequence. *Nucleic Acids Res.*, **37**, 931–938.